Journal of Catalysis 274 (2010) 130–141

Contents lists available at ScienceDirect

Journal of Catalysis

journal homepage: www.elsevier.com/locate/jcat

Immobilization of anionic metalloporphyrins on zinc hydroxide nitrate and study of an unusual catalytic activity

Guilherme S. Machado [a,b], Gregório G.C. Arízaga [c], Fernando Wypych [b], Shirley Nakagaki [a,*]

[a] Universidade Federal do Paraná, Departamento de Química – Laboratório de Bioinorgânica e Catálise – CP 19081, CEP 81531990, Curitiba, Paraná, Brazil
[b] Universidade Federal do Paraná, Departamento de Química – Centro de Pesquisa em Química Aplicada (CEPESQ) – CP 19081, CEP 81531990, Curitiba, Paraná, Brazil
[c] Universidade Federal do Paraná, Departamento de Química – Centro de Nanociencias y Nanotecnologia, Universidad Nacional Autónoma de México, Mexico

ARTICLE INFO

Article history:
Received 22 April 2010
Revised 18 June 2010
Accepted 22 June 2010
Available online 31 July 2010

Keywords:
Iron porphyrin
Catalysis
Zinc hydroxide nitrate
Oxidation
Cyclohexanone

ABSTRACT

This paper is the first report on the immobilization of an anionic iron(III) porphyrin family on zinc hydroxide nitrate (**ZHN**), a layered hydroxide salt. **ZNH** was prepared by means of a precipitation reaction between a zinc nitrate solution and ammonium hydroxide. Two immobilization systems were investigated, namely magnetic stirring at room temperature and stirring/reflux in an ethanolic solution. The solids were characterized by powder X-ray diffraction (XRD), electron paramagnetic resonance (EPR), thermogravimetric and derivative thermogravimetric (TGA/DTG), transmission electron microscopy (TEM), as well as ultraviolet–visible (UV–Vis) and Fourier transform infrared (FTIR) spectroscopic analyses. The catalytic activity of the materials was investigated in the oxidation of cyclooctene, cyclohexane, and *n*-heptane using iodosylbenzene as oxygen donor. The oxidation products were analyzed by gas chromatography. The results revealed an unusual selectivity for cyclohexanone in the reactions of cyclohexane oxidation catalyzed by the anionic iron(III) porphyrins immobilized onto **ZHN**. These results suggest that the structure of the **ZHN** support influences the catalytic mechanism and that cyclohexane oxidation occurs via a radicalar pathway.

1. Introduction

Researchers have great expectations of bioinorganic chemistry because macrocyclic compounds, such as metalloporphyrins, are effective oxidation catalysts [1–3], especially when they are employed as models of biological systems with recognized catalytic activity [4,5]. The cytochrome P450 enzymes have been studied for over 30 years. The large interest in this class of compounds stems from the fact that P450 can act as a monooxygenase, catalyzing the oxidation of organic substrates like drugs and xenobiotics by molecular O_2 in living organisms [1,2]. Synthetic metalloporphyrins, in turn, are able to successfully mimic the activity of cytochrome P450 *in vitro* [4,5].

Countless actual industrial processes require oxidation reactions. One typical example is the manufacture of Nylon 6.6, which involves oxidation of cyclohexane to cyclohexanol and cyclohexanone, for production of adipic acid [6]. In this reaction, a cobalt salt is used as catalyst at a temperature of approximately 150 °C and pressure of 15 bar, but low yields are achieved; *i.e.*, only 5% cyclohexanol and cyclohexanone. In this context, the search for selective, efficient, recyclable catalysts capable of performing oxidation reactions in mild conditions, with high turnover number, continues to represent a challenge for chemistry researchers [1]. In this sense, the utilization of systems inspired on biological enzymes has furnished significant results [7], mainly when biomimetic models immobilized onto different supports are concerned, thereby allowing catalyst recovery and reuse [8–11].

Many studies on the immobilization of a wide variety of metalloporphyrins containing different metals, like manganese or iron, onto inorganic supports, such as natural mineral clays [12–14], synthetic aluminosilicate [8], silica [15], and more recently, synthetic anionic exchangers based on layered compounds like layered double hydroxides [16,17], as well as other solids [18,19], have been reported. After immobilization, metalloporphyrins exhibit higher catalytic efficiency and larger resistance to degradation than their homogeneous counterparts, not to mention their possible reuse, thereby envisaging a future technological application for these catalysts. Another major advantage of catalyst immobilization is related to the enhanced selectivity of the catalytic process [20], or creation of a new selectivity of the catalyst, thus demonstrating the fundamental importance of the support features for the shape-selectivity of the immobilized metalloporphyrin.

In this context, layered materials are an alternative and interesting class of solids for use as inorganic supports. Layered hydroxide salts, which consist of positively charged layers separated by exchangeable anions, are an example of solid that has raised great expectations and stands as a promising support material. There has

* Corresponding author. Fax: +55 41 33613186.
E-mail address: shirley@quimica.ufpr.br (S. Nakagaki).

0021-9517/$ - see front matter © 2010 Elsevier Inc. All rights reserved.
doi:10.1016/j.jcat.2010.06.012

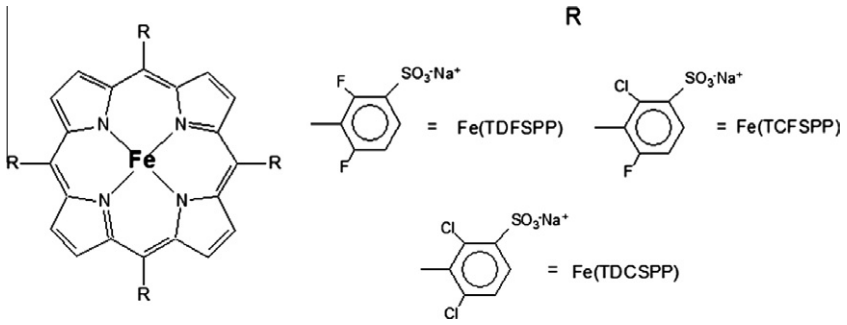

Fig. 1. Structure of the iron porphyrins employed in this study: $[Fe(TDFSPP)Na_4]^+$ = [tetrasodium-5,10,15,20-tetrakis (2,6-difluoro-3-sulfonatophenyl) porphyrinate iron(III)], $[Fe(TCFSPP)Na_4]^+$ = [tetrasodium-5,10,15,20-tetrakis (2-chloro-6-fluoro-3-sulfonatophenyl) porphyrinate iron(III)], and $[Fe(TDCSPP)Na_4]^+$ = [tetrasodium-5,10,15,20-tetrakis (2,6-dichloro-3-sulfonatophenyl) porphyrinate iron(III)].

been great emphasis on the study of these salts over the last years [21–24]; however, the use of this class of compounds as catalysts or inorganic supports has been poorly explored. In fact, to the best of our knowledge, their use as inorganic matrix for metalloporphyrin immobilization had never been described in the literature until the present work. The basic structure of a layered hydroxide salt consists of modified brucite ($Mg(OH)_2$) layers, which in turn are formed by a hexagonal packet of hydroxyl ions where the layer octahedral sites are occupied by an Mg^{2+} metallic center surrounded by hydroxyl groups [22]. These compounds have a basal distance of 4.8 Å in a neutral layered structure [25]. Brucite can be altered in terms of composition: structural Mg^{2+} can be replaced with other ions, such as Zn^{2+}, Co^{2+}, or Cu^{2+} [21,24], while hydroxyl groups can be substituted with other species, like water [21] or nitrate [22]. The latter modification originates the class of layered hydroxide salts, which consist of an alternated sequence of changed brucite-like layers and intercalated anions [22].

The specific class of hydroxide nitrates can adopt two distinct structures [21]. The first refers to the structure of copper hydroxide nitrate, where nitrate ions are directly coordinated to copper atoms, resulting in a solid with a basal space of 6.9 Å. The second structure is represented by the structure of zinc hydroxide nitrate (**ZHN**). In the latter case, the solid layer is formed by zinc octahedra containing one fourth of their sites vacant; while zinc atoms coordinated in tetrahedral geometry are located on the superior and inferior sides of the octahedra. Three vertices of the zinc tetrahedra are occupied by hydroxyl ions from the octahedral sheet, whereas the fourth apical vertex contains a water molecule. The nitrate ions are located between the layers of **ZHN** and are not coordinated to the metal. The basal space of this kind of solid is larger; i.e., approximately 9.9 Å [21,22].

In this work, the immobilization of an anionic iron(III) porphyrin family (Fig. 1) on **ZHN** is reported. Also, an investigation into the catalytic activity of the resulting anionic iron(III) porphyrin–**ZHN** solids in the oxidation of cyclooctene, cyclohexane, and heptane by iodosylbenzene is carried out. The initial purpose of the present work was to try to develop a simple method for the preparation of an efficient and selective heterogeneous catalyst consisting of iron(III) porphyrins immobilized onto **ZHN**. To our surprise, we found out that the obtained catalysts display an unexpected and unusual selectivity in cyclohexane oxidation reactions.

2. Experimental

2.1. Reagents

All chemicals used in this study were purchased from Aldrich, Sigma, or Merck and were of analytical grade. Iodosylbenzene (PhIO) was synthesized by hydrolysis of iodosylbenzenediacetate [26]. The solid was carefully dried under reduced pressure and kept at 5 °C; its purity was periodically controlled by iodometric titration [27].

2.2. Porphyrins and metalloporphyrins

The anionic free base porphyrins $Na_4[H_2(TDFSPP)]$, $Na_4[H_2(TCFSPP)]$, and $Na_4[H_2(TDCSPP)]$ and their corresponding iron(III) porphyrin (FePor) complexes ($[Fe(TDFSPP)Na_4]^+$ = [tetrasodium-5,10,15,20-tetrakis (2,6-difluoro-3-sulfonatophenyl) porphyrinate iron(III)]; ($[Fe(TCFSPP)Na_4]^+$ = [tetrasodium-5,10,15,20-tetrakis (2-chloro-6-fluoro-3-sulfonatophenyl) porphyrinate iron(III)] and ($[Fe(TDCSPP)Na_4]^+$ = [tetrasodium-5,10,15,20-tetrakis (2,6-dichloro-3-sulfonatophenyl) porphyrinate iron(III)]) were synthesized, purified, and characterized following a previously described method [20,28]. For the sake of simplification, these three FePor will be represented in this work by [Fe(TDFSPP)], [Fe(TCFSPP)], and [Fe(TDCSPP)], respectively, so hereafter no mention of the FePor porphyrin charges will be made, to avoid repetition. The Soret bands of the FePor obtained after the metal insertion reaction were the following: [Fe(TDFSPP)] (ethanol) 390 nm ($\varepsilon = 47 \times 10^3$ L mol^{-1} cm^{-1}), [Fe(TCFSPP)] (ethanol) 412 nm ($\varepsilon = 71 \times 10^3$ L mol^{-1} cm^{-1}), and [Fe(TDCSPP)] (ethanol) 390 nm ($\varepsilon = 74 \times 10^3$ L mol^{-1} cm^{-1}).

2.3. Preparation of the heterogeneous catalysts FePor–*ZHN*

A solution with a $Zn(NO_3)_2{\cdot}6H_2O$ concentration of 0.33 mol L^{-1} was prepared in distilled water, kept under magnetic stirring, and heated to approximately 50–60 °C. Drops of an NH_4OH (28%) solution were slowly added to the aforementioned solution, until a white cloudy precipitate of **ZHN** ($Zn_5(OH)_8(NO_3)_2{\cdot}2H_2O$) was formed [21,22]. A total of 5 mL NH_4OH solution was added in the course of 1 h of reaction; the solution pH was analyzed every 5 min, until the pH became neutral.

At the end of the reaction, the suspension containing the **ZHN** solid was centrifuged, and the supernatant was removed. The **ZHN** solid was then washed five times with distilled water and dried in an oven at 50 °C for 48 h. The total reaction yield was 96% in relation to the theoretically predicted amount.

The three FePor [Fe(TDFSPP)], [Fe(TCFSPP)], and [Fe(TDCSPP)] were chosen for immobilization onto the synthesized **ZHN** support. These FePor consist of anionic molecules, so they can easily interact with the positively charged surface of the **ZHN** matrix. Alternatively, the negatively charged FePor can be potentially intercalated between the support layers, thereby replacing nitrate anions.

Two immobilization procedures were investigated in ethanol. The first used magnetic stirring and reflux conditions, while the second employed magnetic stirring at room temperature. For the

immobilization process, 5 mg of one of the FePor was dissolved in 25 mL ethanol and kept under stirring or stirring/reflux. Then, 250 mg of the **ZHN** support was added to the resulting solution. For each FePor, the FePor–**ZHN** suspension was centrifuged after 5 h of reaction, and the respective supernatant was collected in a volumetric flask for further analyses by ultraviolet–visible spectroscopy (UV–Vis). The obtained FePor–**ZHN** solids were washed five times with ethanol, and the corresponding supernatants were also collected in the respective volumetric flasks mentioned above. The resulting colored FePor–**ZNH** solids were air-dried for 48 h and labeled as follows: FeDF–**ZHN**, FeDC–**ZHN**, and FeCF–**ZHN**, for the immobilization of the [Fe(TDFSPP)], [Fe(TDCSPP)], and [Fe(TCFSPP)], into zinc hydroxide nitrate, respectively.

The **ZHN** solid and all the FePor–**ZNH** solids were characterized by powder X-ray diffraction (XRD), Fourier transform infrared (FTIR) spectroscopy, UV–Vis spectroscopy (solids suspended in Nujol mineral oil), transmission electron microscopy (TEM), electron paramagnetic resonance (EPR), and thermogravimetric and derivative thermogravimetric (TGA/DTG).

After use, all reagents were discarded in an appropriate container for later treatment and reuse, or for final disposal.

2.4. Oxidation of cyclooctene, cyclohexane, and n-heptane by PhIO catalyzed by the FePor–*ZHN* solids

The solids obtained by immobilization of the anionic FePor onto the synthetic **ZHN** matrix were used as catalysts in the oxidation reactions. These reactions were carried out in a thermostatic glass reactor (2 mL) equipped with a magnetic stirrer bar [10,13,15]; the catalyst and PhIO were suspended in the solvent mixture (0.300 mL dichloromethane/acetonitrile 1:1 v/v), and the substrate (cyclooctene, cyclohexane, or *n*-heptane) was then added to the reaction mixture, resulting in a constant compound/oxidant/substrate molar ratio of 1:20:2000. The oxidation reaction was allowed to proceed for 1 h, under magnetic stirring. Sodium sulfite was added to the reaction mixture, in order to eliminate excess PhIO and to quench the reaction after the experiment time was over. The reaction products were separated from the FePor–**ZHN** catalyst by centrifugation and transferred to a volumetric flask. Next, the FePor–**ZHN** solid employed in the reaction was washed several times with dichloromethane and acetonitrile, in order to extract any reaction product that might have been retained in the catalyst. The solution containing the final reaction products and the solvents from the washings of the FePor–**ZHN** were analyzed by gas chromatography. Product yields were quantified on the basis of PhIO, and high-purity *n*-octanol (99.9%) (acetonitrile solution, 1.0×10^{-2} mol L^{-1}) was employed as internal standard. Control reactions were carried out using the same procedure in the case of: (a) the substrate, (b) substrate + PhIO, and (c) substrate + PhIO + **ZHN** (without FePor). The corresponding FePor in homogeneous solution were also tested as catalyst (homogeneous catalysis), and the experimental procedure in this case was similar to that utilized the heterogeneous catalysis.

Catalyst reuse tests were also performed for all the substrates. At the end of each reaction, the catalytic solid was separated and washed with water, followed by reflux with acetonitrile and then methanol in a Soxhlet extractor for at least 12 h. All the solvents used in the washing procedure were analyzed by UV–Vis spectroscopy, in order to detect possible lixiviation of the catalyst from the support.

A study was also performed by changing the reaction solvent mixture acetonitrile/dichloromethane 1:1 (v/v) for acetonitrile/dichloroethane 1:1 (v/v) and pure dichloroethane or pure acetonitrile, in order to evaluate the influence of the solvent on product yields and on the selectivity of the cyclohexane catalytic oxidation. Finally, reactions were performed in the presence of a radical scavenger, *tert*-butyl-alcohol [29], used in volumes similar to those employed for the substrate.

2.5. Characterization of the FePor–*ZHN* catalysts

For the XRD measurements, self-oriented films were placed on neutral glass sample holders. XRD patterns were acquired in reflection mode using a Shimadzu XRD-6000 diffractometer operating at 40 kV, 40 mA, and using Cu Kα radiation (λ = 1.5418 Å) and a dwell time of 1°/min.

FTIR spectra were recorded on a Biorad 3500 GX spectrophotometer in the range of 400–4000 cm^{-1}, using KBr pellets. KBr was crushed with a small amount of the solids, and the spectra were collected with a resolution of 4 cm^{-1} and accumulation of 32 scans.

UV–Vis spectra were registered in the 200–800 nm range in an HP 8452A diode array spectrophotometer. Analyses were accomplished with a 1-cm path length cell.

TEM analyses were carried out in a JEOL-JEM 1200–100 kV system, using a drop of powder suspension of the samples deposited on copper grids covered with parlodium.

EPR measurements were performed on a Bruker ESP 300E spectrometer operating at the X-band (approximately 9.5 GHz), at 293 or 77 K, using liquid N_2.

TGA/DTG measurements were carried out on a Thermal Analyst TA Instrument SDT Q 600 Simultaneous DTATG-DSC. The measurements were done under air, at a heating rate of 20 °C/min.

All the products from the catalytic oxidation reactions were identified using a Shimadzu GC-14B gas chromatograph (flame ionization detector) equipped with a 30-m-long DB-WAX capillary column with 0.25 mm internal diameter (J&W Scientific). The oven temperature program used for the determination of the oxidation products from cyclooctene and cyclohexane started at 100 °C; the temperature was increased to 150 °C at 10 °C min^{-1}, followed by further temperature rise to 200 °C at 50 °C min^{-1}, which was maintained for 1 min. For the determination of the products originated from n-heptane, the temperature program started at 80 °C, followed by a temperature elevation to 100 °C at 5 °C min^{-1}, maintained for 1 min, and a further temperature increase to 200 °C at 10 °C min^{-1}, kept for 1 min.

3. Results and discussion

Fig. 2 depicts the XRD patterns of the **ZHN** solid, which has a basal distance of 9.8 Å, characteristic of $Zn_5(OH)_8(NO_3)_2{\cdot}2H_2O$ [30]. The diffraction patterns of the solids obtained after immobilization of [Fe(TDFSPP)] onto **ZHN** using magnetic stirring at room temperature and magnetic stirring at solvent reflux conditions can be observed in Fig. 2b and c, respectively. The pattern in Fig. 2b displays the same typical peaks of the 9.8 Å basal distance present in Fig. 2a, suggesting that immobilization of this FePor onto **ZHN** takes place on the surface of the solid, mainly.

Immobilization of [Fe(TDFSPP)] onto **ZHN** using magnetic stirring/reflux conditions (Fig. 2c) leads to disruption of the **ZHN** structure, originating zinc oxide only [31]. This indicates the low stability of the **ZHN** support in solution at higher temperatures [21,31], where it is gradually decomposed to ZnO. Due to this behavior, FePor immobilization was performed by magnetic stirring at room temperature thereafter. No evidence of any intercalation reactions was observed in the XRD patterns.

The XRD patterns of the solids obtained after immobilization of [Fe(TCFSPP)] and [Fe(TDCSPP] onto **ZNH** are shown in Fig. 2d and e, respectively. Both compounds kept the same basal distance of 9.8 Å observed in the original **ZHN**. Decreased crystallinity was detected for all the FePor–**ZNH** solids, an effect that can be attributed

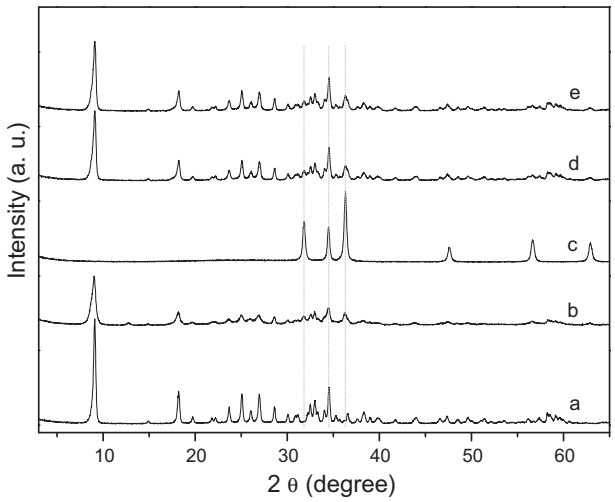

Fig. 2. XRD patterns of the synthesized **ZHN** (a), FeDF–**ZHN** – after stirring only (b), FeDF–**ZHN** – after stirring under reflux conditions (c), FeCF–**ZHN** – after stirring only (d) and FeDC–**ZHN** – after stirring only (e).

Table 1
Rate of FePor immobilization onto the **ZHN** support.

FePor	Supported FePor compounds[a]	Immobilization rate[b] (%)	Loading[c] (mol g^{-1})
[Fe(TDFSPP)]	FeDF–**ZHN**	100	1.7×10^{-5}
[Fe(TCFSPP)]	FeCF–**ZHN**	96	1.6×10^{-5}
[Fe(TDCSPP)]	FeDC–**ZHN**	98	1.5×10^{-5}

[a] Prepared compound nomenclature: e.g. FeDF–**ZHN**; compound resulted by the immobilization of the [Fe(TDFSPP)] on the zinc hydroxide nitrate solid.
[b] Relative to the initial amount of FePor used in the immobilization process.
[c] FePor–**ZHN** (mol g^{-1}).

to crystal fragmentation due to the magnetic stirring bar employed during the immobilization process. The maintenance of the original basal distance of 9.8 Å (the distance of intercalated nitrate) [32] in all the FePor–**ZHN** samples reinforces that FePor immobilization occurred on the surface of the solid, without substantial replacement of the interlayer nitrate ions with FePor anions. Finally, a small contamination with zinc oxide was observed in all the solids.

The immobilization rates and loadings (mol of FePor *per* gram of **ZHN**) were determined by UV–Vis spectroscopy of the prepared solid catalysts supernatants, as summarized in Table 1.

It is expected that FePor immobilization onto **ZHN** should occur via the strong electrostatic interactions between the negative charges of the FePor catalysts and the positively charged surface of the support. These positive charges are present in the solid matrix because of the vacancy of negative charges promoted by the zinc ions in tetrahedral configuration [21]. A possible location of the FePor immobilized onto the **ZHN** support is represented in Fig. 3, where [Fe(TDFSPP)] is used as example. The same hypothesis can also be applied to the other two FePor. The distance between each top of the tetrahedra created by the zinc atom on the **ZHN** structure is approximately 6 Å [30], and the mean size of a metalloporphyrin bearing sulfonate groups is approximately 15 Å [33], which excludes the possibility of FePor intercalation. Another important observation is that there is no possibility of the FePor being allocated in such a way that the four charges of the four sulfonate groups located on the porphyrin ring are neutralized, since FePor interaction with the support surface occurs at a maximum of two points. If the FePor charges were neutralized, the metalloporphyrin center containing the Fe(III) ion would be too close to the positively charged top of the tetrahedron. Therefore, it is reasonable to suppose that the FePor accommodates at the top of the layered crystals, as represented in Fig. 3, where the ring is positioned with a tilted orientation. This arrangement would allow for interaction between at least two anionic groups of the FePor and the tetrahedron tops on the **ZHN** surface, and the metallic centers of the FePor would be far from the support surface. In this configuration, part of the FePor anionic groups could be positioned outside of the surface and protonated or interacting with another layered crystal surface. From the XRD experiments, it is clearly seem that the Fepor anionic species were not intercalated between the **ZHN** layers (Fig. 2).

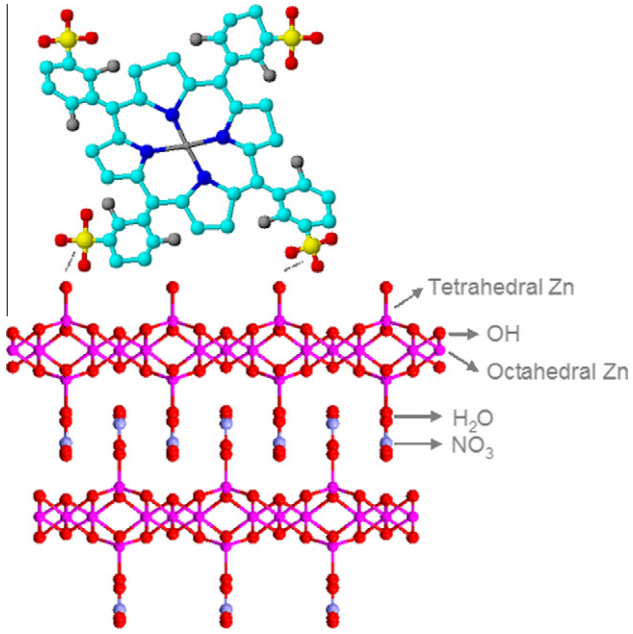

Fig. 3. Schematic representation of the [Fe(TDFSPP)] immobilized on the corrugated surface of **ZHN**. Nitrate ions were removed from the top of the superior layer and from the bottom of the inferior layer, to facilitate visualization.

Fig. 4 shows the FTIR spectra of the solids obtained after immobilization of the FePor onto the **ZHN** support. Attribution of the

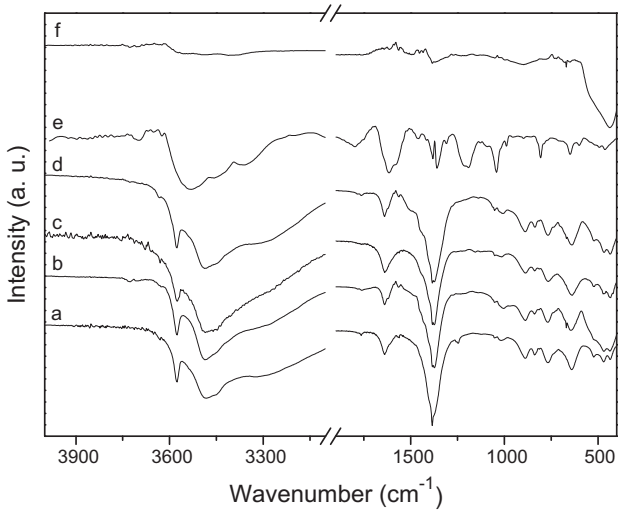

Fig. 4. FTIR spectra of **ZHN** (a), FeDF–**ZHN** (b), FeCF–**ZHN** (c), FeDC–**ZHN** (d), [Fe(TDCSPP)] (e), and [Fe(TDFSPP)]/ZnO (f).

Table 2
ZHN FTIR bands and the respective attributions [21,23,31,34].

Band (cm^{-1})	Attribution
3576	Stretching of OH group linked with the layer
3481	Stretching of OH water group
3313	Stretching of OH group linked with the nitrate
1639	Angular vibration of interlayer water molecules
1384	Asymmetrical stretching of the nitrate ion (v_3) – characteristic for D_{3h} symmetry of nitrate ion – free interlayer nitrate
1016	Symmetrical stretching of the nitrate ion (v_1)
835	Asymmetrical deformation of nitrate ion (v_2)
767	Symmetrical deformation of nitrate ion (v_4)
640, 522, 470	Group of bands for Zn–O vibration

bands present in the FTIR spectrum of the **ZHN** solid (Fig. 4a) is presented in Table 2 [21,23,31,34]. For comparison, Fig. 4f contains the FTIR spectrum of [Fe(TDFSPP)] immobilized onto **ZHN** under magnetic stirring/ reflux conditions which, as discussed for the XRD patterns, consists of ZnO. Only an intense band in the 500 cm^{-1} region can be observed for the latter solid, ascribed to Zn–O vibration [31].

Also for comparison purposes, Fig. 4e displays the FTIR spectrum of pure [Fe(TDCSPP)], where the characteristic FTIR spectrum of a sulfonato-phenyl-substituted porphyrin is shown [13]. There are bands related to the vibration of the SO_3 group at 1100 cm^{-1} and to aromatic C=C bonds near 1600 cm^{-1} [35]. The spectrum in Fig. 4e is similar to those of [Fe(TDFSPP)] and [Fe(TCFSPP)].

Because of the very low concentration of the FePor on the support, the FTIR spectra of FeDF–**ZHN** (Fig. 4b), FeCF–**ZHN** (Fig. 4c), and FeDC–**ZHN** (Fig. 4d) are dominated by the intense bands of the **ZHN** matrix. The only evidence of the presence of the FePor on the supports is the different color of the solid achieved after the immobilization process, since pure **ZHN** is white.

It was possible to demonstrate the presence of the immobilized FePor in the FePor–**ZHN** solids by UV–Vis spectroscopy (Fig. 5). The UV–Vis spectra of FeDF–**ZHN**, FeCF–**ZHN**, and FeDC–**ZHN** are represented in Fig. 5b–d, respectively, where the characteristic Soret band of each immobilized FePor can be seen. When these spectra are compared with those of the parent pure FePor in Nujol mull, a red-shift of the Soret band is observed for [Fe(TDFSPP)] (414 nm) and [Fe(TCFSPP)] (422 nm) [14]. This effect had already been reported for other immobilized metalloporphyrins [13,18] and can be attributed to the interaction between the complex and the surface of the solid support, which can impose steric limitations to the immobilized metalloporphyrin [36]. The immobilization process creates a larger distortion of the porphyrin ring, so the porphyrin a_{2u} orbital (HOMO orbital – highest occupied molecular orbital) is closer to the e_g orbital (LUMO orbital – lowest unoccupied molecular orbital) [37]. This distortion and the consequent shorter distance between the orbitals result in a red-shifted Soret band [38]. As for [Fe(TDCSPP)] (416 nm), with larger substituents in the ortho-phenyl positions of the porphyrin ring, the macrocyclic ring is less distorted, so there is no appreciable shift of the Soret band when the maximum absorbance bands of the pure [Fe(TDCSPP)] (416 nm) and the immobilized [Fe(TDCSPP)] (418 nm) are compared. Fig. 5a presents the UV–Vis spectrum of pure **ZHN**, where no bands in the region where the FePor absorb can be detected, thereby confirming that the bands observed in the UV–Vis spectra of the FePor–**ZHN** are really due to the presence of the FePor complexes.

Fig. 6 shows the EPR spectra of the FePor–**ZHN** solids synthesized in this work. The EPR-silent spectrum of **ZHN** (Fig. 6a) indicates that the prepared FePor–**ZHN** solids are free of paramagnetic species that could have been inserted into the support by the primary reactants or during the synthetic process. For the solids FeDF–**ZHN** (Fig. 6b), FeCF–**ZHN** (Fig. 6c), and FeDC–**ZHN** (Fig. 6d), the signal attributed to high-spin Fe(III) in axial symmetry, $g = 5.8$, is observed, which is typical of the presence of Fe(III) in the FePor complex [39,40]. A signal in $g = 4.3$ can also be seen, which can be assigned to high-spin Fe(III) in rhombic symmetry [39,41]. Fig. 6e–g corresponds to the EPR spectra of the pure [Fe(TDFSPP)], [Fe(TCFSPP)], and [Fe(TDCSPP)], respectively. In these spectra, there is an intense signal at $g_{\perp} = 5.8$ as well as a signal in $g_{//} = 2.0$, characteristic of high-spin Fe(III) ($S = 5/2$) in axial symmetry, as frequently observed in pure FePor [39]. A low intensity signal in $g = 4.3$ can also be observed, which is ascribed to high-spin Fe(III) in rhombic symmetry [14,40]. The intensity of this signal increases in the spectra of the FePor–**ZHN** solids. As reported in other works [14,42,43], this suggests that the interaction between the FePor and the surface of the support can promote distortion in the total conformation of the FePor molecule, thereby changing the axial symmetry of the metallic center to the rhombic symmetry. Compared with FeDC–**ZHN**, the rise in the signal corresponding to rhombic high-spin Fe(III) is more pronounced for FeDF–**ZHN** and FeCF–**ZHN**. This is probably because in the former case, the presence of the chlorine atoms in the phenyl rings of

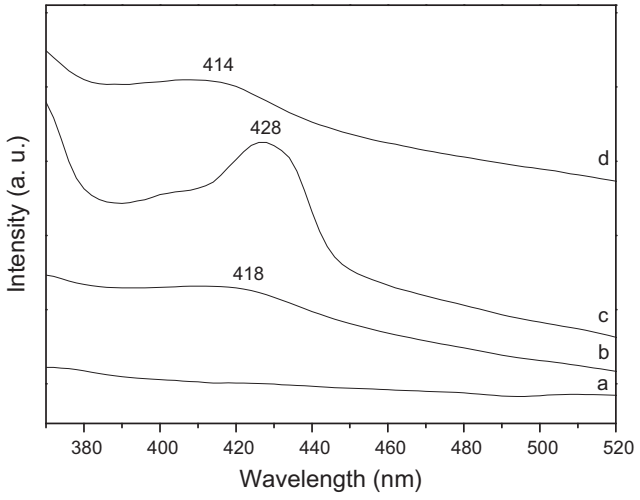

Fig. 5. UV–Vis spectra of **ZHN** (a), FeDF–**ZHN** (b), FeCF–**ZHN** (c), and FeDC–**ZHN** (d).

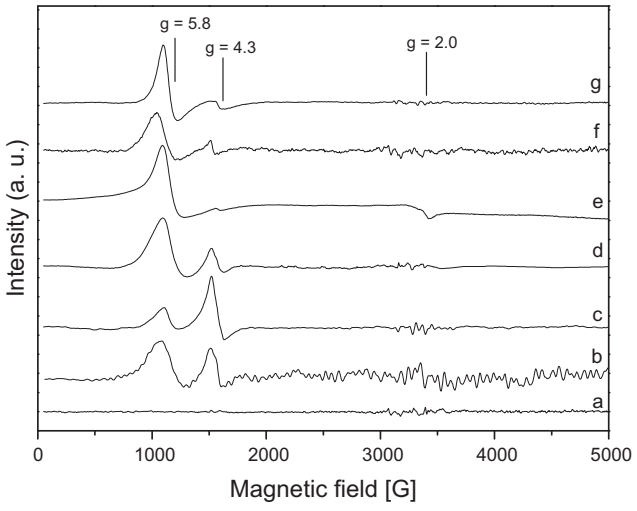

Fig. 6. EPR spectra of **ZHN** (a), FeDF–**ZHN** (b), FeCF–**ZHN** (c), FeDC–**ZHN** (d), [Fe(TDFSPP)] (e), [Fe(TCFSPP)] (f), and [Fe(TDCSPP)] (g).

the FePor promotes less distortion in the immobilized FePor, so that the majority of the Fe(III) remains in axial symmetry. This corroborates the above discussion on the UV–Vis spectroscopy of FeDC–**ZHN**, where the displacement of the Soret band obtained after immobilization of [Fe(TDCSPP)] onto **ZHN** was shown to be only very discrete.

TGA/DTG analysis was used to characterize the **ZHN** solid (Fig. 7). The observed mass loss of 35.6% is very close to the expected theoretical value of 34.7%, for $Zn_5(OH)_8(NO_3)_2{\cdot}2H_2O$ [31]. The loss of adsorbed water molecules and hydration water molecules takes place at 200 °C, with a mass loss of approximately 11.6%, leading to the formation of the $Zn_3(OH)_4(NO_3)_2$ species [31]. At 300 °C, the mass loss related to the decomposition of $Zn_3(OH)_4(NO_3)_2$ to $Zn(NO_3)_2$ occurs. Finally, the latter compound decomposes to ZnO when it is heated at temperatures higher than 300 °C [30,31]. The DTG curve (Fig. 7b) reveals the presence of three main decomposition processes in the sample, with maximum endothermic peaks at 150, 187, and 297 °C. As for FeDF–**ZHN**, FeCF–**ZHN**, and FeDC–**ZHN**, the mass losses (data not shown) were 34.3%, 34.3%, and 34.1%, respectively, which disagrees with the amount of organic matter corresponding to the quantity of FePor immobilized onto the support (around 2%). Because FePor immobilization occurs mainly on the surface of the support, FePor molecules can be occupying positions previously taken by nitrates or water molecules on the surface, thereby influencing the amount of mass loss achieved in the analysis.

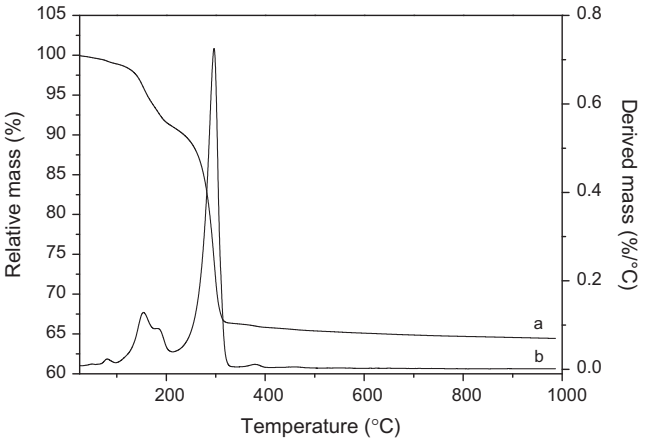

Fig. 7. TGA/DTG analyses of **ZHN**.

The morphology of the FePor–**ZHN** solids was examined by TEM (Fig. 8). The growth of the solid crystals follows a pseudo-orthorhombic orientation [21], with three different axes *a*, *b*, and *c*, and angles between them are close to 90°, thereby originating morphologies resembling rectangles. Fig. 8a shows the micrograph of the **ZHN** support, which contains tabular crystals and is comparable with morphologies of other synthesized hydroxide salts reported in the literature [23]. Additionally, it can be noticed that crystal growth is oriented toward the formation of rectangles, with some corners close to 90°. The **ZHN** crystals have width between 0.5 μm and 1 μm, and length of approximately 2 μm. Moreover, this solid is relatively uniform, which is in good agreement with the intense diffraction peaks observed in the XRD patterns (Fig. 2). Fig. 8b–d displays the micrographs of FeDF–**ZHN**, FeCF–**ZHN**, and FeDC–**ZHN**, respectively. In all the cases, the relative size of the crystals is smaller compared with that of pure **ZHN**, suggesting that crystal fragmentation occurred during the immobilization process. This size reduction is responsible for the lower peak intensities observed in the XRD analyses. With respect to FePor immobilization, structure fragmentation is interesting because it

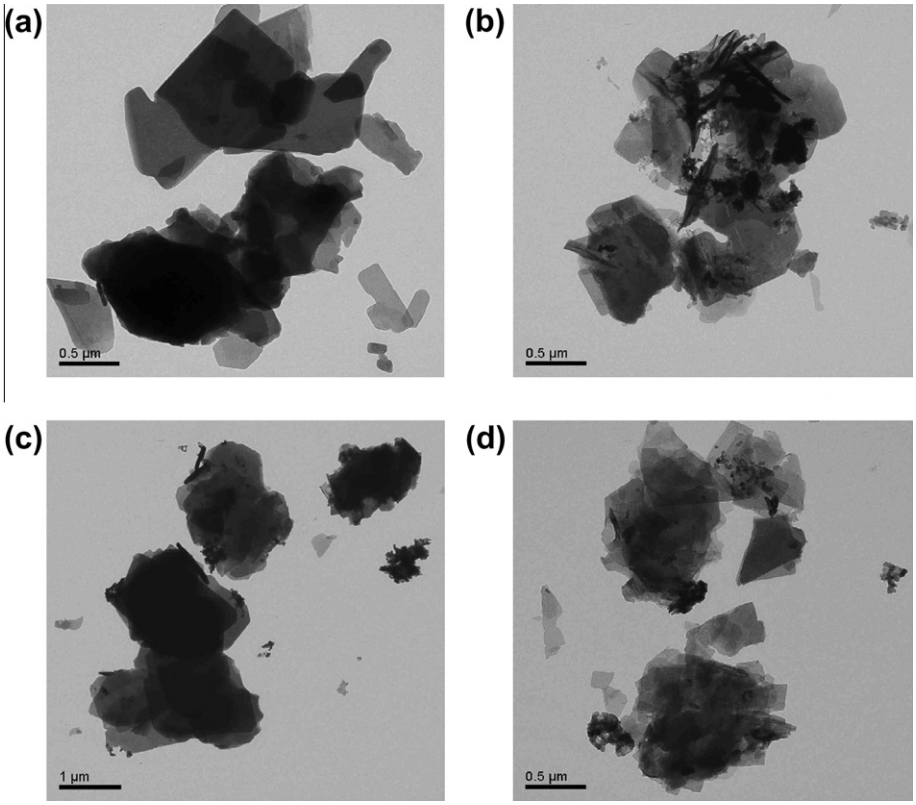

Fig. 8. TEM of **ZHN** (a), FeDF–**ZHN** (b), FeCF–**ZHN** (c), and FeDC–**ZHN** (d).

imparts an increase in the surface area, thus facilitating the interaction between the solid support and the FePor.

The catalytic activity of the prepared solids was first evaluated in the oxidation of cyclooctene, which is more easily oxidized and is a well-known diagnostic substrate for the evaluation of catalytic activity (Table 3) [13]. In fact, cyclooctene is a reactive alkene that is frequently employed in investigations involving homogeneous and heterogeneous catalysis [16,18,40,42,43]. Only cyclooctenoxide is observed as the final reaction product when metalloporphyrins are employed as catalyst, which is attributed to the high stability of the active intermediate radical species generated from the metalloporphyrin during the oxidation reaction. Concerning FePor, a high catalytic efficiency is usually observed in the oxidation of cyclooctene catalyzed by these complexes, since this alkene is easy to oxidize This fact is probably related to the generation of the active catalytic species ferryl porphyrin π-cation radical $Fe^{IV}(O)P^{\cdot+}$, which is very reactive toward the double bonds of cyclic alkenes [4,44,45].

The best cyclooctenoxide yields were achieved in the reactions employing the supported FePor catalysts (Table 3 – Runs 1, 3, and 5), which were higher than the results obtained with the parent FePor in solution (homogeneous catalysis – Table 3 – Runs 7–9). Among all the catalysts, FeDC–**ZHN** furnished the best product yield: about 100% cyclooctenoxide was obtained. This fact can be related to the way that [Fe(TDCSPP)] is immobilized onto the support. The characterization of this solid, already described above, suggests that there is a more superficial interaction of this FePor with the **ZHN** solid. Hence, the FePor active site must be more accessible to the reactants in FeDC–**ZHN**, leading to better catalytic activity compared with the other solids. Stronger FePor–**ZHN** interactions and thus larger metallocomplex distortions were observed for the other two FePor by EPR analysis; however, both still gave good catalytic results in the case of cyclooctene oxidation.

The advantage of using supported catalysts is the possibility of multiple reuses [5,10,11]. So, after the first use, the FePor–**ZHN** solids were recovered by filtration, washed, and used again in another cyclooctene oxidation reaction. The reused catalysts (Table 3 – Runs 2, 4, and 6) furnished slightly decreased product yields. No FePor lixiviation from the support during the washing procedure was detected by UV–Vis spectroscopy, so this decrease cannot be attributed to the loss of FePor, but to a possible deactivation of some active catalytic species. Nonetheless, the yields of the reused heterogeneous catalysts were still superior to those achieved with homogeneous catalysis, thereby demonstrating the advantage of the immobilization process. Finally, the control reactions using the oxidant only (PhIO – Table 3 – Run 10) and the **ZHN** support with no FePor + oxidant (Table 3 – Run 11) resulted in low catalytic yields, thereby confirming that the catalytic efficiency of the FePor–**ZHN** solids is really due to the FePor.

Next, the prepared solids were studied as catalysts in the oxidation of less reactive, saturated hydrocarbons [10,20,40,46]. Cyclohexane was chosen as the saturated substrate, because it is relatively inert and there are many successful catalytic examples discussed in the literature [4,42,46]. This substrate enables investigation into the catalytic efficiency and selectivity of the catalytic species since two major products can be observed, namely cyclohexanol and cyclohexanone. Another reason for studying the catalytic oxidation of cyclohexane is the industrial importance of its oxidation products. Moreover, the search for cheaper and more efficient catalysts that can work in mild conditions is still a challenge for chemical researchers [1].

The results obtained for the oxidation of cyclohexane catalyzed by the immobilized FePor–**ZHN** (Table 4 – Runs 12, 14, and 16) showed that these solids are efficient catalysts, with total yields comparable or superior to those achieved with the homogeneous counterparts (Table 4 – Runs 18–20). In the case of FeCF–**ZHN** (Table 4 – Run 14), the total yield is lower than the homogeneous catalysis with [Fe(TCFSPP)] (Table 4 – Run 19). It is a frequent behavior observed for this iron porphyrin immobilized in different supports. In homogeneous catalysis, one *ortho*-chlorine substituent in each *meso*-phenyl porphyrin groups in the Fe(TCFSPP) can avoid molecular interactions, which can deactivate (by destruction or dimerization of the iron porphyrin) and/or avoid the catalytic active species formation. Therefore, higher yields in oxidation reactions are expected for this iron porphyrin in homogeneous catalysis [18]. In contrast, after immobilization, better catalytic results are observed for Fe(TDFSPP) and Fe(TDCSPP) that could be due to an easy access of PhIO and substrate to the iron sites. In spite of that, the result is comparable with the total yield of the reactions. As in the case of cyclooctene oxidation reactions, FeDC–**ZHN** (Run 16) was more catalytically efficient than the other two FePor–**ZHN**. This suggests that the way the FePor are immobilized onto the **ZHN** support influences the catalytic activity of the FePor–**ZHN** solids, especially considering that the catalytic activities of the three FePor in solution are similar.

It is noteworthy that the three FePor–**ZHN** solids prepared in this work exhibited unusual selectivity for cyclohexanone. Immo-

Table 3
Cyclooctenoxide yields achieved in the oxidation of cyclooctene by PhIO catalyzed by FePor and FePor–**ZHN**.[a]

Catalyst	Run	Cyclooctenoxide yield[b] (%)
FeDF–**ZHN**	1	90
1st reuse	2	81
FeCF–**ZHN**	3	88
1st reuse	4	77
FeDC–**ZHN**	5	98
1st reuse	6	89
[Fe(TDFSPP)]	7	65
[Fe(TCFSPP)]	8	60
[Fe(TDCSPP)]	9	73
PhIO only, no catalyst	10	10
ZHN without immobilized FePor	11	16

[a] Reaction conditions: reactants molar ratio 1:20:2000 (FePor/PhIO/substrate), at room temperature under argon and 1 h of reaction. Homogeneous catalyses were performed under identical conditions to those employed for heterogeneous catalyses.
[b] Yield based on starting PhIO.

Table 4
Oxidation of cyclohexane by PhIO catalyzed by FePor and FePor–**ZHN**.[a]

Catalyst	Run	Alcohol yield[b] (%)	Ketone yield[b] (%)	Total yield (%)	Ketone/alcohol ratio[c]
FeDF–**ZHN**	12	<1	35	36	35
1st reuse	13	3	25	28	
FeCF–**ZHN**	14	<1	23	24	23
1st reuse	15	2	15	17	
FeDC–**ZHN**	16	2	70	72	35
1st reuse	17	5	55	60	
[Fe(TDFSPP)]	18	19	7	26	0.37
[Fe(TCFSPP)]	19	29	4	33	0.14
[Fe(TDCSPP)]	20	31	5	36	0.16
PhIO only, no catalyst	21	<1	<1	1	1
ZHN without immobilized FePor	22	1	1	1	1

[a] Reaction conditions: reactants molar ratio 1:20:2000 (FePor/PhIO/substrate), at room temperature under argon and 1 h of reaction. Homogeneous catalyses were performed under identical conditions to those employed for heterogeneous catalyses.
[b] Yield based on starting PhIO (it was assumed that 2 mols of PhIO were used for ketone formation).
[c] Selectivity for ketone formation in relation to alcohol formation.

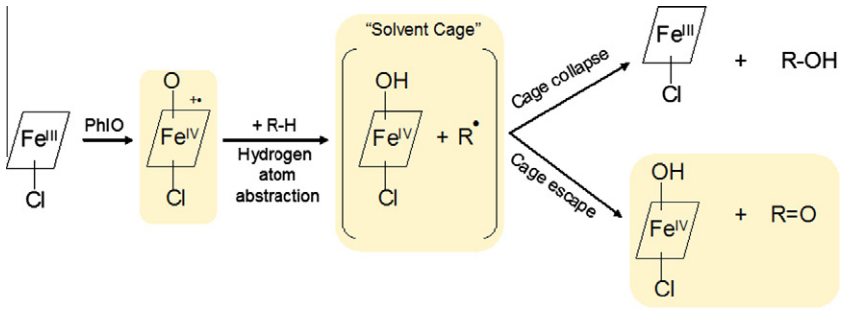

Fig. 9. Cyclohexane oxidation mechanism with FePor as catalyst [42].

bilized FePor catalytic systems are generally selective for cyclohexanol [11,14], as observed in homogenous catalysis. Considerable investigation into the intermediate catalytic species of FePor has shown that the active species generated in oxidation reactions catalyzed by FePor systems consists of a species denominated ferryl porphyrin π-cation, also designated oxo-iron-IV porphyrin radical $(Fe^{IV}{=}O)^{\cdot+}$ [4,44]. The mechanistic studies involving FePor have suggested that after formation of the active catalytic species via interaction between FePor and PhIO, there is hydrogen abstraction from the C–H bond of the substrate, generating a new intermediate species [Fe^{IV}–OH + R·], where R refers to the substrate [4,42]. Cyclohexanol and/or cyclohexanone production depends directly on the formation of this new species. If the recombination of the OH fragment linked to the iron finds the radical formed by the substrate (R· species), cyclohexanol is formed. But if this recombination does not occur rapidly enough, the R· radical species escape from the vicinity of the intermediate species (solvent cage), leading to the formation of other products, such as cyclohexanone (Fig. 9) [42,47]. In fact, some examples in the literature [48–50] have identified radicals being formed at the substrate, with consequent radicalar mechanisms furnishing other products that would not be expected for the conventional catalysis using the FePor model for cytochrome P450. An example is when the reaction occurs in the chlorinated solvents, where reaction products containing chlorine are observed [51].

In general, the use of immobilized FePor has been shown to lead to reaction mechanisms similar to those occurring in solution, and selectivity for the alcohol has been observed in the oxidation of cyclohexane catalyzed by heterogeneous catalysts based on FePor [1,8,10–15,40,52]. In the present work, the fact that selectivity for the ketone was obtained with the solid FePor–**ZHN** catalysts suggests that the catalysts resulting from the immobilization of the FePor onto **ZHN** impair the control of the [Fe^{IV}–OH + R·] species and the relative reaction rates (recombination or radical escape) [42], inasmuch as the homogenous catalysis in the same conditions displayed different selectivity (Table 4 – Runs 18–20). These results are a strong evidence of the influence of the support on the selectivity of the reaction. The surface of the **ZHN** solid is not flat; in fact, there are corrugations associated with the presence of zinc tetrahedra above and below the surface layer [21]. As the analyses of the FePor–**ZHN** solids carried out by us suggest, FePor is predominantly immobilized onto the surface of **ZHN**, and the complex/support environment created by this interaction might make OH transfer to the substrate difficult, thereby causing radical escape and consequent generation of a radicalar oxidative route to cyclohexanone. This behavior is not observed for other immobilized FePor systems employing the same FePor utilized in the present work; for instance, when natural mineral clays [12–14], layered double hydroxides [16,17], and silica [15] are used as support. In the latter systems, the solid surface tends to be more uniform and flatter compared to the surface of **ZHN**. In fact, when our research group investigated the catalytic activity of [Fe(TDFSPP)] immobilized onto a nitrate-intercalated layered double hydroxide surface, only cyclohexanol was produced (8% yield); that is, no cyclohexanone was detected under the same catalytic conditions.

Apart from ketone production by radical escape, this product can be frequently formed by re-oxidation of the alcohol product present in the vicinity of the active catalytic species in a second oxidation cycle [4]. When heterogeneous catalysts are employed, the escape of the alcohol formed in a selective catalytic reaction from the active site can be hampered by the structure of the catalyst. In these cases, the alcohol concentration in the vicinity of the catalytic species increases, so this product becomes a new substrate for a further oxidation reaction [53].

In order to investigate whether cyclohexanone formation could be due to further alcohol oxidation [1,4], tests of the catalytic activity of FeDF–**ZHN** were conducted using different reaction times (Table 5). After 15 min of reaction (Table 5 – Run 23), 30% cyclohexanone yield could already be observed, with traces of cyclohexanol product only. Prolonging the reaction time to 30 and 45 min (Table 5 – Runs 24 and 25, respectively), 33% and 34% cyclohexanone yields were respectively obtained, without any apparent increase in the cyclohexanol yield. This same behavior was observed after 1, 24, and 48 h of reaction (Table 5 – Runs 26, 27 and 28, respectively), when 35%, 43%, and 48% cyclohexanone yields were, respectively, achieved. Therefore, the majority of cyclohexanone was produced within the first 15 min of reaction, accompanied by traces of cyclohexanol only. Prolonged reaction times resulted in higher cyclohexanone yield with minimal increase in cyclohexanol yield. Taken together, these observations reinforce the fact that ketone production is independent of alcohol production and suggest that a radicalar reaction mechanism is responsible for ketone production. The same behavior was observed for reaction times shorter than 15 min.

In order to investigate which factors interfere in the oxidation of cyclohexane in the presence of the heterogeneous catalysts FePor–**ZHN**, a reaction was performed using [Fe(TDFSPP)] immobilized on

Table 5
Oxidation of cyclohexane by PhIO catalyzed by FeDF–**ZHN** carried out with variable time.[a]

Run	Time (h)	Alcohol yield[b] (%)	Ketone yield[b] (%)
23	0.25	<1	30
24	0.5	<1	33
25	0.75	<1	34
26	1	<1	35
27	24	1	43
28	48	2	48

[a] Reaction conditions: reactants molar ratio 1:20:2000 (FePor/PhIO/substrate), at room temperature under argon.
[b] Yield based on starting PhIO (it was assumed that 2 mol of PhIO were used for ketone formation).

zinc oxide as catalyst, which was obtained by thermal decomposition in **ZHN** solution. In this case, the cyclohexanol and cyclohexanone yields were 40% and only 2%, respectively. The zinc oxide derived from the hydroxide salt no longer has the layered, corrugated structure observed for **ZHN** [21]. Taken together, all these results strongly indicate that the environment created by FePor immobilization onto **ZHN**, which has an irregular surface, really influences the catalytic route in the case of cyclohexane oxidation, favoring the major production of cyclohexanone.

Next, the oxidation of cyclohexane was investigated in different solvents, in order to check the influence of the reaction medium composition (Table 6) on product yields [10,51,54]. In the acetonitrile/dichloroethane solvent system ($CH_3CN/C_2H_4Cl_2$, Table 6 – Runs 30, 33, and 36), the product yields obtained with the three FePor–**ZHN** were slightly lower compared with those of the reactions performed in the acetonitrile/dichloromethane solvent system (CH_3CN/CH_2Cl_2, Table 6 – Runs 29, 32, and 35). In the former case, the decreased total yields can be attributed to the viscosity and the different solubility of the reactants in the new solvent system [51]. In general, the more viscous a solvent, the longer the lifetime of the intermediate species inside the "solvent cage". The viscosity of the solvents used here are 0.779, 0.413, and 0.343 mPa s for dichloroethane, dichloromethane, and acetonitrile, respectively [55], so dichloroethane is the most viscous. The reduced production of cyclohexanone in the presence of dichloroethane can be explained by the change in medium viscosity, which results in slightly increased alcohol production, although the system is still more selective for the ketone [51]. In the case of pure dichloroethane (Table 6 – Runs 31, 34, and 37), reduced cyclohexanone and larger cyclohexanol production can also be detected for the three FePor–**ZHN** catalysts. The selectivity for ketone is thus maintained in all the employed solvent systems, suggesting that the support structure is responsible for the elevated selectivity toward cyclohexanone formation, despite the influence of the solvent on product yields and reaction selectivity.

Concerning the results presented in Table 4, the reactions using the reused FePor–**ZHN** catalysts (Table 4 – Runs 13, 15, and 17) evidenced slightly lower total yields compared to the fresh catalyst. However, the amount of cyclohexanol obtained with the reused catalysts was larger, with consequent decreased reaction selectivity toward cyclohexanone. The reduced product yields in the presence of the reused catalysts, also observed in the case of cyclooctene oxidation, can be accounted for deactivation of some of the FePor active sites on the surface of the support [10] or decomposition to ZnO, the last hypothesis could not be proven by the small amount of solid used in the catalytic tests. The deactivation can be explained by the oxidizing action of the reaction medium, but it is smaller compared to the deactivation observed in the case of homogeneous catalysis.

As for the control reactions using only the oxidizing agent (Table 4 – Run 21) and the oxidant together with the **ZHN** support without FePor (Table 4 – Run 22), low cyclohexanol and cyclohexanone yields were obtained, confirming that the catalytic activity is really due to the FePor complexes.

Finally, the FeDC–**ZHN** solid (Table 4 – Run 16) furnished higher cyclohexanone yield compared with the other two FePor–**ZHN** catalysts (Table 4, FeDF–**ZHN** – Run 12, and FeCF–**ZHN** – Run 14). This behavior can be due to the structure of the FePor and to how it is immobilized onto the **ZHN** support. The [Fe(TDCSPP)] complex contains two chlorine atoms on each phenyl substituent on the porphyrin ring. Because chlorine is bulkier than the fluorine atoms on [Fe(TDFSPP)] and [Fe(TCFSPP)], they may prevent the establishment of a strong interaction between the FePor complex and the surface of the support, thereby facilitating interaction of the catalyst active site with the substrate and the oxidant present in the reaction medium, which would justify the larger cyclohexanone production. In the case of the two other FePor, their more effective interaction with the support might hinder the access of the oxidant and the substrate to the FePor center, leading to lower product yields compared with FeDC–**ZHN**.

Linear alkanes are more resistant to oxidation compared to cyclic alkenes and alkanes [11,13,20,52,56], and only rarely have catalytic systems capable of oxidizing the former substrates been reported to furnish appreciable product yields [10,11,56,57]. Furthermore, the oxo-functionalization of the terminal position of linear alkenes is a big challenge [13]. In fact, few literature works describe the selective oxidation of linear alkanes at position 1, or even position 2 [56,57]. The dissociation energy of linear C–H bonds in alkanes decreases in the order 104, 95.3, and 91 kcal mol^{-1} for primary, secondary, and tertiary carbons, respectively [56]. This is the reason why the vast majority of works on the catalytic oxidation of linear alkanes report oxidation at positions 2 and 3 of the carbon chain [10,11,13,50]. In the catalytic oxidation of heptane catalyzed by the three FePor–**ZHN** prepared in this work (Table 7 – Runs 38, 40 and 42), there was selective production of heptanol. As generally observed for cyclic alkanes, most of the FePor catalysts generate alcohol as the main product of the oxidation of linear alkanes [11,13]. The mechanism through which product formation occurs has already been discussed above [4]. In our case, because a high selectivity for the ketone had been obtained in the oxidation of cyclohexane catalyzed by FePor–**ZHN**, we had also expected such selectivity in the case of heptane oxidation, which did not occur. A possible explanation for that may be related to the different structures of the substrates cyclohexane and heptane. Apart from having a cyclic structure, cyclohexane can be present in two different conformations; that is, "chair" or "boat" [10]. These factors can influence the reaction rate and the recombination or escape of the radical formed in the [Fe^{IV}–OH + R·] species [4]. As for the linear heptane [20,52], such structural rearrangements do not occur during formation of the intermediate species, mainly because of the irregularities present on the surface of the support. So the alcohol should be preferentially formed via the classical mechanism described for alkane oxidation catalyzed by FePor. Although the catalyst reuse reactions (Table 7 – Runs 39, 41, and 43) evidenced reduced catalytic efficiency, the fact that the FePor–**ZHN** are still active in a second reaction demonstrates that the heterogeneous catalysts are advantageous compared to the parent homogenous catalysts [10]. Nevertheless, one might still argue that the product yields furnished by the heterogeneous

Table 6
Oxidation of cyclohexane by PhIO catalyzed by FePor and FePor–**ZHN** carried out for 1 h, in distinct solvent systems.[a]

Catalyst	Run	Solvent system	Cyclohexanol yield[b] (%)	Cyclohexanone yield[b] (%)
	29	CH_3CN/CH_2Cl_2[c]	<1	35
FeDF–**ZHN**	30	$CH_3CN/C_2H_4Cl_2$[d]	4	23
	31	$C_2H_4Cl_2$[e]	5	19
	32	CH_3CN/CH_2Cl_2	<1	23
FeCF–**ZHN**	33	$CH_3CN:C_2H_4Cl_2$	3	16
	34	$C_2H_4Cl_2$	4	14
	35	CH_3CN/CH_2Cl_2	2	70
FeDC–**ZHN**	36	$CH_3CN/C_2H_4Cl_2$	5	49
	37	$C_2H_4Cl_2$	7	43

[a] Reaction conditions: reactants molar ratio 1:20:2000 (FePor/PhIO/substrate), at room temperature under argon. Homogeneous catalyses were performed under identical conditions to those employed for heterogeneous catalyses.
[b] Yield based on starting PhIO (it was assumed that 2 mol of PhIO were used for ketone formation).
[c] Solvent system: acetonitrile/dichloromethane, 1:1 (v/v).
[d] Solvent system: acetonitrile/dichloroethane, 1:1 (v/v).
[e] Solvent system: pure dichloroethane.

Table 7
Oxidation of *n*-heptane by PhIO catalyzed by FePor and FePor–**ZHN** carried out for 1 h.[a]

Catalyst	Run	Heptane oxidation products yield[b] (%)									
		1-ol[c]	2-ol[c]	3-ol[c]	4-ol[c]	Total ol	2-one[d]	3-one[d]	4-one[d]	Total one	Ol/one[e]
FeDF–**ZHN**	38	3	5	12	2	22	–	1	1	2	11
1st reuse	39	3	4	10	1	18	–	2	–	2	9
FeCF–**ZHN**	40	1	2	9	1	13	1	1	1	3	4.3
1st reuse	41	1	1	5	–	8	–	–	–	–	8
FeDC–**ZHN**	42	2	5	15	3	25	–	2	1	3	8.3
1st reuse	43	2	–	12	2	16	–	–	2	2	8
[Fe(TDFSPP)]	44	–	30	–	–	30	–	12	–	12	2.5
[Fe(TCFSPP)]	45	–	17	–	–	17	–	5	–	5	3.4
[Fe(TDCSPP)]	46	–	39	–	–	39	–	15	–	15	2.6
PhIO only, no catalyst	47	–	–	–	–	–	–	–	–	–	–
ZHN	48	–	–	–	–	–	–	–	–	–	–

[a] Reaction conditions: reactants molar ratio 1:20:2000 (FePor/PhIO/substrate), at room temperature under argon. Homogeneous catalyses were performed under identical conditions to those employed for heterogeneous catalyses.
[b] Yield based on starting PhIO.
[c] Heptanol.
[d] Heptanone.
[e] Selectivity for alcohol formation in relation to ketone formation.

catalysts were lower than those achieved by homogenous catalysis (Table 7 – Runs 44–46). However, in homogeneous medium, there was selectivity for alcohol formation at position 2 and ketone formation at position 3 of the carbon chain, demonstrating that the lower selectivity of the FePor in solution compared to those of the FePor–**ZHN** catalysts is a major drawback. A factor that frequently influences changes in product selectivity is the steric factor. In homogeneous solution, only the steric factors related to the structure of the FePor itself operate [57], whereas the interaction established between the FePor and the support is decisive for the selectivity of the heterogeneous catalyst [11,12]. Steric factors are extremely important for catalytic reactions because they can change the physical access of the substrate to the active catalytic species formed in the metallic center, thereby determining reaction selectivity.

It is worth mentioning that, as reported for the other substrates employed in this work, control reactions using heptane (Table 7 – Runs 47 and 48) also demonstrated that in the absence of the FePor, no product is observed, nor is any hepthaldeide produced.

Finally, in order to demonstrate that cyclohexane oxidation with PhIO catalyzed by the FePor–**ZHN** catalysts prepared in this work really follows a radicalar route, substrate oxidation reactions were performed in the presence of the *radical scavenger tert*-butyl alcohol [29,58], which is largely employed in the literature to verify whether radicalar pathways evolve during intermediate steps of the reaction [59,60]. Other compounds, such as hydroquinone [61] and 2-methyl-2-nitropropane [62], can also be used as radical scavengers. Besides that, the *radical scavenger* bromotrichloromethane ($BrCCl_3$) can be also used for a better identification of radicalar route and the product bromocyclohexane can be expected [51]. *Radical scavengers* compete with the substrate in radicalar reaction mechanisms and are preferentially oxidized, thereby avoiding formation of products derived from radicals generated from the main substrate [58,60]. The consequence is a reduction in the product yields, which is a proof that substrate oxidation really follows a radicalar route [59]. In the case the reaction follows a radicalar path, *tert*-butyl alcohol is oxidized to 2-propanone mainly [63].

Table 8 summarizes the results obtained in the oxidation of cyclooctene, cyclohexane, and heptane in both the presence and the absence of *tert*-butyl alcohol. With respect to the oxidation of cyclooctene and heptane, the results achieved in the presence and in the absence of the *radical scavenger* were very similar; there was only a small increase in the total product yield for both substrates in reactions carried out in the presence of *tert*-butyl alcohol. These results strongly suggest that the mechanism is not governed by a radical route in the case of the oxidation of cyclooctene and heptane catalyzed by FePor–**ZHN**, and the oxidation products are mainly obtained by action of the oxo-iron-IV porphyrin radical $(Fe^{IV}{=}O)^{\cdot+}$ [4,44]. On the other hand, different results were achieved for the oxidation of cyclohexane in the presence and absence of the *radical scavenger*. There was a drastic reduction in product yield in the presence of *tert*-butyl alcohol compared to

Table 8
Oxidation reaction of cyclooctene, cyclohexane, and *n*-heptane with PhIO catalyzed by FePor and FePor–**ZHN** carried out for 1 h in the presence and absence of a *radical scavenger* (*tert*-butyl alcohol).[a,b]

Catalyst	Condition	C-oxide[c] (%)	C-ol[d] (%)	C-one[e] (%)	H-ol total[f] (%)	H-one total[g] (%)
FeDF–**ZHN**	Without *tert*-butyl-alcohol	90	<1	35	22	2
FeCF–**ZHN**		88	<1	23	13	3
FeDC–**ZHN**		98	2	70	25	3
FeDF–**ZHN**	With *tert*-butyl-alcohol	94	2	2	27	4
FeCF–**ZHN**		90	2	3	17	1
FeDC–**ZHN**		98	2	4	28	3

[a] Reaction conditions: reactants molar ratio 1:20:2000 (FePor/PhIO/substrate), at room temperature under argon. When the reaction was performed in the presence of the radical scavenger, 50 μL of *tert*-butyl alcohol was added to each reaction vessel.
[b] Yield based on starting PhIO.
[c] Cyclooctenoxide.
[d] Cyclohexanol.
[e] Cyclohexanone.
[f] Heptanol.
[g] Heptanone.

the product yields obtained in the absence of the *scavenger*. Cyclohexanone production was strongly affected in the presence of *tert*-butyl alcohol, which has larger affinity for the active catalytic species than the cyclohexane radicals. The sharp decrease in total product yield in the case of cyclohexane oxidation catalyzed by FePor–**ZHN** in the presence of the *radical scavenger* is strong evidence that the oxidation reaction mechanism follows a radical route [42,59]. Besides that, in the cyclohexane oxidation reaction performed in dichloromethane/acetonitrile solvent mixture, a small peak in the retention time of 1.77 was also observed in GC analysis that was identified as chloro-cyclohexane product. In a catalysis carried only in pure acetonitrile, this peak was not observed. The presence of the chlorinated product also suggests that a radicalar reaction mechanism is occurring [64].

In conclusion, the obtained results show that the effective combination between the irregular surface of the **ZHN** support and the immobilized FePor creates a singular environment that provides new selectivity for porphyrin systems in the case of the catalytic oxidation of cyclohexane. Moreover, the reaction mechanism probably consists of a radical route.

4. Conclusions

The inorganic support **ZHN** was obtained by precipitation in controlled pH and characterized by various instrumental techniques. The immobilization of a family of anionic iron porphyrins was performed by magnetic stirring in ethanolic solution at room temperature, with good rates of complex immobilization onto **ZHN**. The supported catalysts prepared here were analyzed by many techniques, which suggested that the iron porphyrins were immobilized on the surface of **ZHN**. The catalytic activity of the iron porphyrins immobilized on **ZHN** was evaluated in the oxidation of organic substrates with PhIO. The immobilized catalysts were efficient, as evidenced from the cyclooctene oxidation reactions. An interesting and surprising selectivity for cyclohexanone was observed in the case of cyclohexane oxidation. As for heptane oxidation, selectivity for heptanol and higher 3-heptanol yields were achieved.

The catalytic results suggest the involvement of a radical mechanism for the cyclohexane oxidation reaction, where the control of the active catalytic species can be influenced by the irregular surface of the support and by the cyclic structure of the substrate. Indeed, such selectivity for the ketone was not observed for heptane, a linear alkane. The influence of the **ZHN** corrugated surface was confirmed by studies involving [Fe(TDFSPP)] immobilized on zinc oxide, which showed selectivity for the alcohol during cyclohexane catalytic oxidation, and not for the ketone. As far as the immobilized catalysts employed in this work are concerned, the solvent used in the reaction also contributes to the higher selectivity for cyclohexanone. When pure 1,2-dichloroethane was used, the selectivity for cyclohexanone decreased compared with an acetonitrile/dichloromethane 1:1 (v/v) solvent mixture. Finally, reactions conducted in the presence of the *radical scavenger tert*-butyl alcohol strongly suggest that the oxidation of cyclohexane catalyzed by the FePor–**ZHN** follows a radical route. The reused supported catalysts also exhibited good catalytic efficiency in the oxidation of the three substrates.

To the best of our knowledge, this is the first time that **ZHN** has been used as support for the immobilization of metalloporphyrins. The methodology employed here for the synthesis of supported catalysts can be very interesting, because the support is cheap, easily obtained, is based on highly available and non-toxic elements, and displays different selectivity. The results from cyclohexane oxidation reactions showed how the support can modify the catalytic behavior of a certain species, making the rational planning of various immobilized catalysts onto different inorganic supports a very interesting approach for the design of a new and wide range of catalysts.

Acknowledgments

The authors thank Conselho Nacional de Desenvolvimento Científico e Tecnológico (CNPq), Coordenação de Aperfeiçoamento de Pessoal de Nível Superior (CAPES), Fundação Araucária, Fundação da Universidade Federal do Paraná (FUNPAR), and Universidade Federal do Paraná (UFPR) for financial support. The authors are also grateful to Centro de Microscopia Eletrônica da UFPR for the TEM analyses. G.S. Machado thanks CAPES for a master grant.

References

[1] D. Mansuy, C. R. Chim. 10 (2007) 392.
[2] K.S. Suslick, in: K. Kadish, K. Smith, R. Guillard (Eds.), The Porphyrin Handbook, Academic Press, New York, 1999, p. 1.
[3] A.J. Appleton, S. Evans, J.R.L. Smith, J. Chem. Soc. Perkin Trans. 2 (1995) 281.
[4] J.T. Groves, J. Inorg. Biochem. 100 (2006) 434.
[5] F. Bedioui, Coord. Chem. Rev. 144 (1995) 39.
[6] F.A. Chavez, J.M. Rowland, M.M. Olmstead, P.K. Mascharak, J. Am. Chem. Soc. 120 (1998) 9015.
[7] R. Song, A. Robert, J. Bernadou, B. Meunier, Inorg. Chim. Acta 272 (1998) 228.
[8] G.S. Machado, K.A.D.F. Castro, O.J. Lima, E.J. Nassar, K.J. Ciuffi, S. Nakagaki, Colloids Surf. A 349 (2009) 162.
[9] K.S. Suslick, P. Bhyrappa, J.H. Chou, M.E. Kosal, S. Nakagaki, D.W. Smithenry, S.R. Wilson, Acc. Chem. Res. 38 (2005) 283.
[10] S. Nakagaki, G.S. Machado, M. Halma, A.A.S. Marangon, K.A.D.F. Castro, N. Mattoso, F. Wypych, J. Catal. 242 (2006) 110.
[11] L. Barloy, J.P. Lallier, P. Battioni, D. Mansuy, Y. Piffard, M. Tournoux, J.B. Valim, W. Jones, New J. Chem. 16 (1992) 71.
[12] G. Huang, T. Li, S. Liu, M. Fan, Y. Jiang, Y. Guo, Appl. Catal. A 371 (2009) 161.
[13] G.S. Machado, K.A.D.F. Castro, F. Wypych, S. Nakagaki, J. Mol. Catal. A: Chem. 283 (2008) 99.
[14] M. Halma, A. Bail, F. Wypych, S. Nakagaki, J. Mol. Catal. A: Chem. 243 (2006) 44.
[15] M.S.M. Moreira, P.R. Martins, R.B. Curi, O.R. Nascimento, Y. Iamamoto, J. Mol. Catal. A: Chem. 233 (2005) 73.
[16] M. Halma, F. Wypych, S.M. Drechsel, S. Nakagaki, J. Porphyr. Phthalocya. 6 (2002) 502.
[17] Z. Tonga, T. Shichia, K. Takagi, Mater. Lett. 57 (2003) 2258.
[18] S. Nakagaki, K.A.D.F. Castro, G.S. Machado, M. Halma, S.M. Drechsel, F. Wypych, J. Braz. Chem. Soc. 17 (2006) 1672.
[19] J. Xie, Y. Wang, Y. Wei, Catal. Commun. 11 (2009) 110.
[20] S. Nakagaki, F.L. Benedito, F. Wypych, J. Mol. Catal. A: Chem. 217 (2004) 121.
[21] G.G.C. Arízaga, K.G. Satyanarayana, F. Wypych, Solid State Ionics 178 (2007) 1143.
[22] G.G.C. Arizaga, A.S. Mangrich, J.E.F.C. Gardolinski, F. Wypych, J. Colloid Interf. Sci. 320 (2008) 168.
[23] M. Xue, R. Chitrakar, K. Sakane, K. Ooi, S. Kobayashi, M. Ohnishi, A. Doi, J. Solid State Chem. 177 (2004) 1624.
[24] C. Henrist, K. Traina, C. Hubert, G. Toussaint, A. Rulmont, R. Cloots, J. Cryst. Growth 254 (2003) 176.
[25] E.L. Crepaldi, J.B. Valim, Quim. Nova 21 (1998) 300.
[26] J.G. Sharefkin, H. Saltzmann, Org. Synth. 43 (1963) 65.
[27] J.S. Lindsey, I.C. Schreiman, H.C. Hsu, P.C. Kearney, A.M. Marguerettaz, J. Org. Chem. 52 (1987) 827.
[28] A. Adler, F.R. Longo, W. Shergalis, J. Am. Chem. Soc. 86 (1964) 3145.
[29] K.J. Ciuffi, E.J. Nassar, L.A. Rocha, Z.N. Rocha, S. Nakagaki, G. Mata, R. Tujillano, M.A. Vicente, S.A. Korili, A. Gil, Appl. Catal. A 319 (2007) 153.
[30] W. Stählin, H.R. Oswald, Acta Crystallogr. B26 (1970) 860.
[31] T. Biswick, W. Jones, A. Pacula, E. Serwicka, J. Podobinski, J. Solid State Chem. 180 (2007) 1171.
[32] S.P. Newman, W. Jones, J. Solid State Chem. 148 (1999) 26.
[33] M. Halma, K.A.D.F. Castro, C. Taviot-Gueho, V. Prévot, C. Forano, F. Wypych, S. Nakagaki, J. Catal. 257 (2008) 233.
[34] S. Music, D. Dragcevic, S. Popovic, J. Alloys Compd. 429 (2007) 242.
[35] M. Mukherjee, A.R. Raya, J. Mol. Catal. A: Chem. 266 (2007) 207.
[36] H. Kameyama, H. Suzuki, A. Amano, Chem. Lett. 7 (1988) 1117.
[37] L.R. Milgrom, The Colours of Life, Oxford University Press, New York, 1997, p. 85.
[38] M. Gouterman, J. Mol. Spectrosc. 6 (1961) 138.
[39] V. Schünemann, A.X. Trautwein, I.M.C.M. Rietjens, M.G. Boersma, C. Veeger, D. Mandon, R. Weiss, K. Bahl, C. Colapeitro, M. Piech, R.N. Austin, Inorg. Chem. 38 (1999) 4901.
[40] M.A. Schiavon, Y. Iamamoto, O.R. Nascimento, M.D. Assis, J. Mol. Catal. A: Chem. 174 (2001) 213.
[41] C. Piovezan, K.A.D.F. Castro, S.M. Drechsel, S. Nakagaki, Appl. Catal. A 293 (2005) 97.

[42] A.T. Papacídero, L.A. Rocha, B.L. Caetano, E. Molina, H.C. Sacco, E.J. Nassar, Y. Martinelli, C. Mello, S. Nakagaki, K.J. Ciuffi, Colloids Surf. A 275 (2006) 27.
[43] J.T. Groves, W.J. Kruper, J. Am. Chem. Soc. 101 (1979) 7613.
[44] W. Nam, Acc. Chem. Res. 40 (2007) 522.
[45] J.T. Groves, T.E. Nemo, R.S. Myers, J. Am. Chem. Soc. 101 (1979) 1032.
[46] J.P. Collman, H. Tanaka, R.T. Hembre, J.I. Brauman, J. Am. Chem. Soc. 112 (1990) 3689.
[47] M. Fontecave, D. Mansuy, Tetrahedron 40 (1984) 4297.
[48] P. Inchley, J.R. Lindsay-Smith, R.J. Lower, New J. Chem. 13 (1989) 669.
[49] R. Davydov, T.M. Makris, V. Kofman, D.E. Werst, S.G. Sligar, B.M. Hoffman, J. Am. Chem. Soc. 123 (2001) 1403.
[50] K. Auclaire, Z. Hu, D.M. Little, P.R. Ortiz de Montellano, J.T. Groves, J. Am. Chem. Soc. 124 (2002) 6020.
[51] J.R.L. Smith, Y. Iamamoto, F.S. Vinhado, J. Mol. Catal. A: Chem. 252 (2006) 23.
[52] M.A. Martinez-Lorente, P. Battioni, W. Klemiss, J.F. Bartoli, D. Mansuy, J. Mol. Catal. A: Chem. 113 (1996) 343.
[53] S. Nakagaki, C.R. Xavier, A.J. Wosniak, A.S. Mangrich, F. Wypych, M.P. Cantão, I. Denicolo, L.T. Kubota, Colloids Surf. A 168 (2000) 261.
[54] Y. Iamamoto, M.D. Assis, K.J. Ciuffi, H.C. Sacco, L. Iwamoto, A.J.B. Melo, O.R. Nascimento, C.M.C. Prado, J. Mol. Catal. A: Chem. 109 (1996) 189.
[55] CRC Handbook of Chemistry and Physics, 89th ed., 2009, p. 175.
[56] M.J. Thomas, R. Raja, G. Sankar, R.G. Bell, Acc. Chem. Res. 34 (2001) 191.
[57] B.R. Cook, T.J. Reinert, K.S. Suslick, J. Am. Chem. Soc. 108 (1986) 7281.
[58] T.M. El-Morsi, M.M. Emara, H.M.H. Abd El Bary, A. Abd-El-Aziz, K.J. Friesen, Chemosphere 47 (2002) 343.
[59] L.N. Andrade, N. Bizaia, B.L. Caetano, M.L.A. Silva, W.R. Cunha, A.A.S. Filho, P.S. Calefi, E.J. Nassar, J.K. Bastos, K.J. Ciuffi, Catal. Commun. 10 (2009) 669.
[60] K.A. Hislop, J.R. Bolton, Environ. Sci. Technol. 33 (1999) 3119.
[61] S. Lee, R. Raja, K.D.M. Harris, J.M. Thomas, B.F.G. Johnson, G. Sankar, Angew. Chem. Int. Ed. 42 (2003) 1520.
[62] L.B. Luo, D.Y. Han, Y. Wu, X.Y. Song, H.L. Chen, J. Chem. Soc. Perkin Trans. 27 (1998) 1709.
[63] M.N. Schuchmann, C. Sonntag, J. Phys. Chem. 83 (1979) 780.
[64] J.T. Groves, W.J. Kruper, R.C. Haushalter, J. Am. Chem. Soc. 102 (1980) 6377.